

CHAPTER 5

RESULTS OF THE DE HOOP SPELEOTHEM ANALYSES

5.1 Introduction

Since the 1970s speleothems have been used to understand past environmental conditions with palaeo-proxies such as growth laminations, trace elements and stable isotopes derived from these cave deposits (*e.g.* Bar-Matthews *et al.* 1997; Dorale *et al.* 1998; Holmgren *et al.* 1999; Holzkämper *et al.* 2005; McDermott *et al.* 2006; Zhou *et al.* 2008).

This study uses stable carbon and oxygen isotope records preserved in the stalagmites and flowstone sampled from caves in the De Hoop Nature Reserve to generate data regarding the region's palaeoenvironment. The speleothem proxy archive was then dated using the uranium series $^{230}\text{Th}/^{234}\text{U}$ disequilibrium method. The activity ratios of the Th and U isotopes were in turn measured using inductively coupled plasma mass spectrometry techniques (discussed in Chapter 4).

This chapter comprises three sections and reports the results of the U-series dating and stable isotope analyses. The first section focuses on the U-series data. The second part presents the stable isotope results and outlines the steps used to construct an isotope time-series curve. This curve would allow for comparisons between the De Hoop isotope results and other proxy records. The chapter concludes with a summary of the results.

5.1 Uranium series (U-series) age determinations

A chronology for the De Hoop speleothems was established using U-series dates. Based on the selection criteria outlined in section 4.4.2 of Chapter 4 twenty-four subsamples were spiked and prepared for dating (Table 5.1).

Table 5.1 Calculated sample and spike masses including the stratigraphic position of the subsamples represented by the De Hoop stalagmites sampled from Bloukrantz Cave (*Blou1*) and Kaisers Gat II (*KG2.1, KG2.2 & KG2.3*)

Sample name	Lab. No.	Stratigraphic position of the subsample (mm from the top)	Error (mm)	Subsample (g)	Spike (g)
Blou1.1	809	0-5	3.54	0.7620	0.1076
Blou1.2	810	20-27	4.95	0.5007	0.1340
Blou1.3	811	79-85	4.24	0.4980	0.1096
Blou1.4	812	136-150	9.90	0.7440	0.1004
Blou1.5	813	5-10	3.54	0.4392	0.1144
Blou1.6	814	15-19	2.83	0.3900	0.1156
Blou1.7	815	36-40	2.83	0.2404	0.1123
Blou1.8	816	55-60	3.54	0.3110	0.1146
KGII-3.1	817	0-5	3.54	0.3735	0.1035
KGII-3.2	818	10-15	3.54	0.2726	0.1071
KGII-3.3	819	20-25	3.54	0.2679	0.1077
KGII-3.4	820	35-40	3.54	0.3278	0.1058
KGII-3.5	821	50-55	3.54	0.3472	0.1052
KGII-3.6	822	70-75	3.54	0.3799	0.1114
KGII-3.7	823	89-95	4.24	0.4442	0.0860
KGII-3.8	824	119-125	4.24	0.6961	0.1037
KGII-3.9	825	145-150	3.54	0.6480	0.1041
KGII-3.10	826	155-160	3.54	0.6977	0.1077
KGII-3.11	827	190-195	3.54	0.4530	0.1054
KGII-3.12	828	200-209	6.36	0.7708	0.0504
KGII-2.1	829	0-4	2.82	0.2289	0.1032
KGII-2.2	830	6-9	2.12	0.1242	0.1059
KGII-2.3	831	19-24	3.53	0.1486	0.1055
KGII-2.4	832	28-34	4.24	0.1772	0.0974
KGII-2.5	833	46-52	4.24	0.8265	0.1020

The subsamples 813, 814, 815 and 816 representing *Blou1* were lost during the analysis. Additionally, five of the initial 24 subsamples (Lab. No. 823, 826 & 828 to 830) were rejected because of substantial Th contamination and are omitted from the table below (Table 5.2). Under ideal conditions, speleothem carbonate

should contain almost no thorium as ^{230}Th will only be produced over time through the decay of ^{234}U . The resulting $^{230}\text{Th}/^{232}\text{Th}$ ratio is therefore expected to be quite large. As discussed in Chapter 5, thorium is incorporated into the speleothem calcite when it becomes adsorbed onto clay minerals and other detritus and can cause contamination. The adsorption of this detrital ^{230}Th is thought to occur at a constant rate, which in this study was assumed to be 1.5. This value is often referred to as the 'earth mean' and is generally used to measure the $^{230}\text{Th}/^{232}\text{Th}$ activity ratio in a contaminated sample (e.g. Schwarcz *et al.* 1980). During ICP MS analysis ^{230}Th contamination is considered significant when the measured $^{230}\text{Th}/^{232}\text{Th}$ activity ratio is < 50 .

The uranium content (^{238}U) of the remaining 15 subsamples ranged from 0.14 to 0.41 ppm. This was sufficient for ICP MS analysis (see Chapter 4 section 4.4.2). Thorium contamination in these samples was too low to affect the age determinations (based on the measured $^{230}\text{Th}/^{232}\text{Th}$ ratios, which are > 50) (Table 5.2). The corrected ages presented in Table 5.3 are therefore not very different from the ages presented in Table 5.2

Table 5.2 Uranium series disequilibrium data for the De Hoop stalagmites from Bloukrantz Cave and Kaisers Gat II

Sample Id.	Lab. No.	^{238}U ppm ^a	$(^{234}\text{U}/^{238}\text{U})_0$ ^b	$(^{230}\text{Th}/^{234}\text{U})$	$(^{230}\text{Th}/^{232}\text{Th})$	Age (ka) ^c	+2 σ Error (ka) ^d	-2 σ Error (ka)	Initial $(^{234}\text{U}/^{238}\text{U})_0$ ^e
Bloul.1	809	0.3655 (0.0001)	2.887 (0.0946)	0.0324 (0.0042)	114	3.58	0.480	0.478	2.906 (0.0027)
Bloul.2	810	0.4074 (0.0001)	3.262 (0.1038)	0.3567 (0.7213)	13247	45.5	0.390	0.389	3.574 (0.0037)
Bloul.3	811	0.2947 (0.0001)	2.869 (0.1354)	0.3664 (0.6099)	4708	47.1	0.345	0.344	3.137 (0.0042)
Bloul.4	812	0.2750 (0.0001)	2.521 (0.1267)	0.3702 (0.4352)	13252	47.8	0.252	0.252	2.742 (0.0034)
KGII-3.1	817	0.3392 (0.0001)	1.541 (0.0069)	0.6885 (0.0070)	1948	115.5	2.036	1.999	1.751 (0.0079)
KGII-3.2	818	0.3843 (0.0001)	1.541 (0.0115)	0.6654 (0.0086)	745	109.2	2.405	2.351	1.737 (0.0130)
KGII-3.3	819	0.4127 (0.0001)	1.496 (0.0122)	0.6801 (0.0165)	444	113.7	4.769	4.574	1.648 (0.0137)
KGII-3.4	820	0.3032 (0.0001)	1.504 (0.1179)	0.6646 (0.0093)	730	109.4	2.628	2.563	1.687 (0.0132)
KGII-3.5	821	0.2964 (0.0001)	1.500 (0.0081)	0.6547 (0.0113)	2125	106.8	3.047	2.967	1.677 (0.0091)
KGII-3.6	822	0.2891 (0.0001)	1.495 (0.0126)	0.6635 (0.0086)	785	109.2	2.431	2.373	1.674 (0.0142)
KGII-3.8	824	0.1354 (0.0000)	1.470 (0.0072)	0.6490 (0.0155)	1398	105.7	4.163	4.018	1.634 (0.0081)
KGII-3.9	825	0.1726 (0.0000)	1.468 (0.0078)	0.6645 (0.0118)	1430	109.8	3.284	3.191	1.639 (0.0087)
KGII-3.11	827	0.1785 (0.0000)	1.427 (0.0110)	0.6377 (0.0076)	582	103.2	2.070	2.027	1.572 (0.0122)
KGII-2.3	831	0.1404 (0.0000)	1.456 (0.0442)	0.3730 (0.1136)	149	49.4	20.36	17.34	1.525 (0.0463)
KGII-2.4	832	0.2116 (0.0000)	1.503 (0.0146)	0.3256 (0.0223)	515	41.9	3.485	3.383	1.566 (0.0152)

Table 5.3 Corrected uranium series ages for the De Hoop stalagmites

Sample Id.	Lab. No.	Age (ka) ^c	+2σ Error (ka) ^d	-2σ Error (ka)	Initial (²³⁴ U/ ²³⁸ U) ^e	Corrected Age (ka) ^f	+2σ Error (ka)	-2σ Error (ka)	Corrected Initial (²³⁴ U/ ²³⁸ U) ^g
Blou1.1	809	3.58	0.480	0.478	2.906 (0.0027)	3.53	0.480	0.478	2.906 (0.0027)
KGII-3.2	818	109.2	2.405	2.351	1.737 (0.0130) ^d	109.1	2.405	2.351	1.737 (0.0130)
KGII-3.3	819	113.7	4.769	4.574	1.648 (0.0137)	113.5	4.770	4.575	1.648 (0.0137)
KGII-3.4	820	109.4	2.628	2.563	1.687 (0.0132)	109.3	2.628	2.563	1.687 (0.0132)
KGII-3.6	822	109.2	2.431	2.373	1.674 (0.0142)	109.1	2.430	2.373	1.674 (0.0142)
KGII-3.11	827	103.2	2.070	2.027	1.572 (0.0122)	103.1	2.070	2.027	1.572 (0.0122)
KGII-2.3	831	49.4	20.36	17.34	1.525 (0.0463)	49.0	20.37	17.34	1.525 (0.0463)
KGII-2.4	832	41.9	3.485	3.383	1.566 (0.0152)	41.8	3.485	3.383	1.566 (0.0152)

a = ²³⁸U concentration in parts per million (ppm) determined by dissolution (see Chapter 4 section 4.4.2)

b = The measured activity ratio for (²³⁴U/²³⁸U)_o

c = The ICP MS age determination expressed in thousand years (ka)

d = The two σ errors (in parenthesis) (95 % confidence interval)

e = Initial (²³⁴U/²³⁸U) activity ratio

f = Age corrections (ka) used to account for contamination by detrital thorium (²³⁰Th). Assuming a (²³²Th/²³⁰Th) activity ratio of 1.5 (see Chapter 4 section 4.4.2)

g = Corrected initial (²³⁴U/²³⁸U) ratio based on the corrected ages (described in f above)

Speleothem calcite is typically deposited in such a way that younger layers usually overlie the older ones (see Chapter 4 section 4.4.2). Changes in calcite deposition may occur because of detrital material if the speleothems are porous and when the carbonate is re-precipitated (as discussed in Chapter 4). One possible explanation for the age-depth discrepancy in the KG2.3 sample may be related to post-depositional leaching of U. An alternative is that the sequence may be upside down (Fig. 5.1).

The age sequence of sample *KG2.3* appears to be truncated with regards to the stratigraphy with the U-series derived dates increasing in the direction of growth from 103 ka to 115.5 ka. As a result, the sample appears to be older at the top than the bottom (Fig. 5.2). Most of the values however tend to cluster at *c.* 109 ka which may suggest that the apparent inversion represents the natural ‘noise’ in this particular sample.

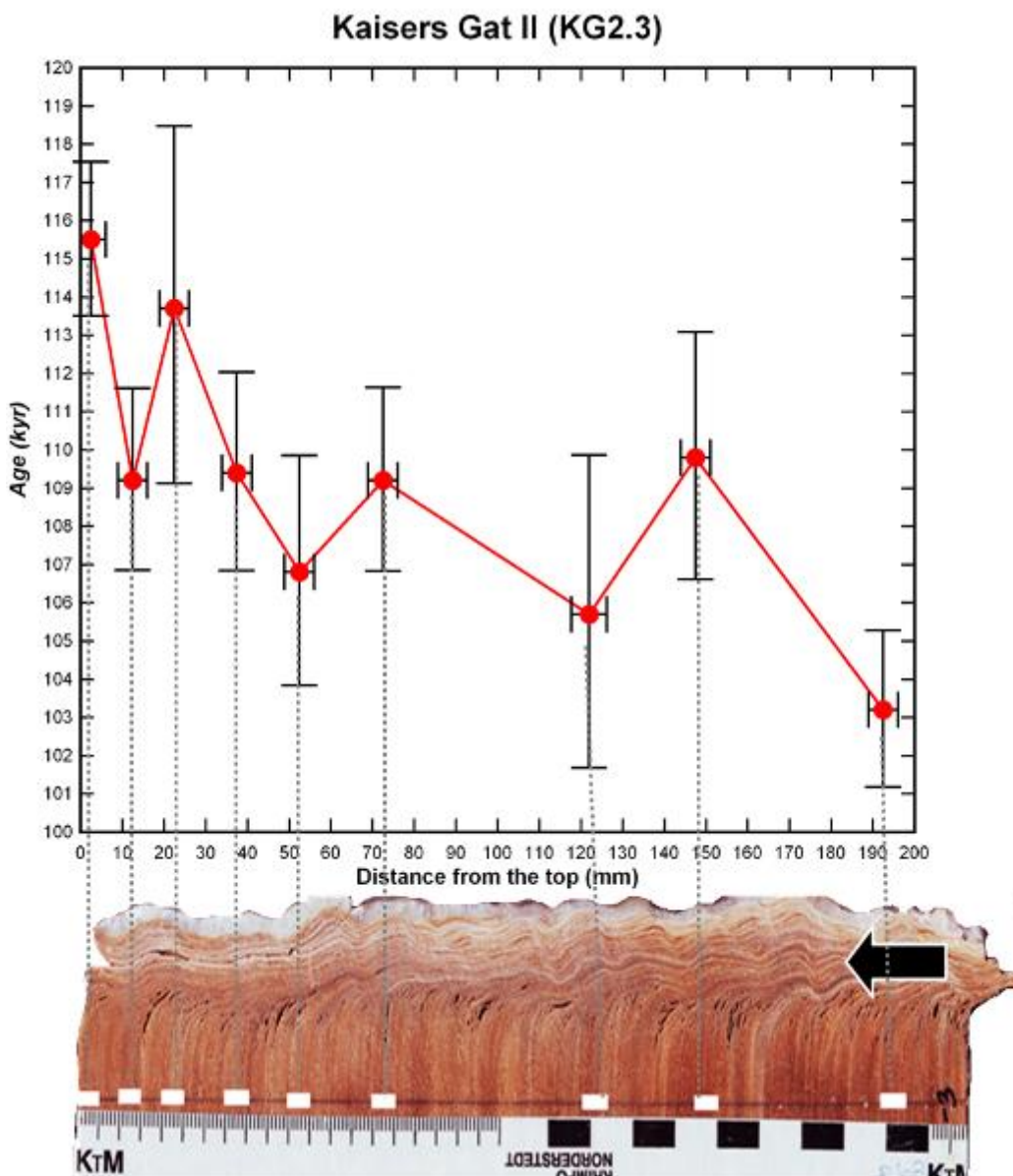


Figure 5.1 Age-depth profile for sample *KG2.3* from the Kaisers Gat II Cave using the stratigraphic data and ages presented in tables 5.1 and 5.2, respectively. The U-series sample locations are represented by white blocks and the arrow indicates the assumed direction of growth

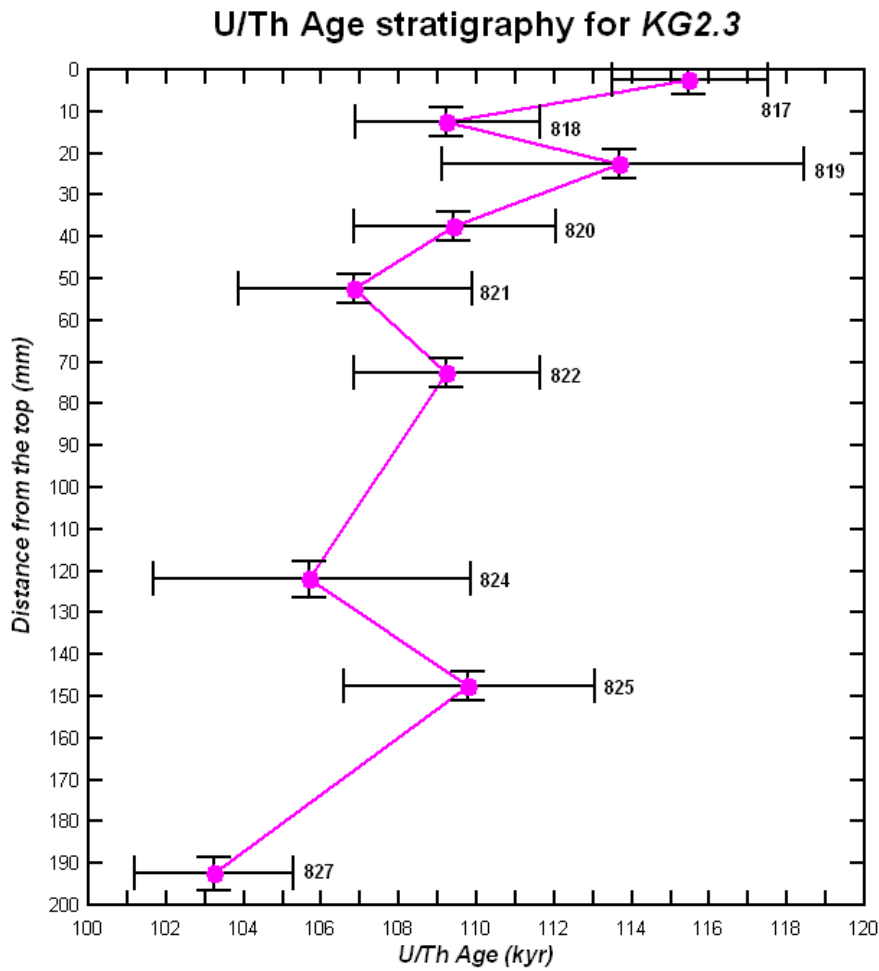


Figure 5.2 Inverted age-depth profile of the *KG2.3* stalagmite and the corresponding sample numbers

As a first approach the $^{234}\text{U}/^{238}\text{U}$, $^{230}\text{Th}/^{234}\text{U}$ and $^{230}\text{Th}/^{232}\text{Th}$ ratios were compared to identify possible leaching. The values (> 750) obtained for the $^{230}\text{Th}/^{232}\text{Th}$ activity ratios across all the *KG2.3* subsamples are substantially higher than the baseline of 50. The latter value is typically used to correct for Th contamination in samples dated using the ICP MS technique (see Chapter 5 section 5.5). This implies that Th contamination in this sample was minimal.

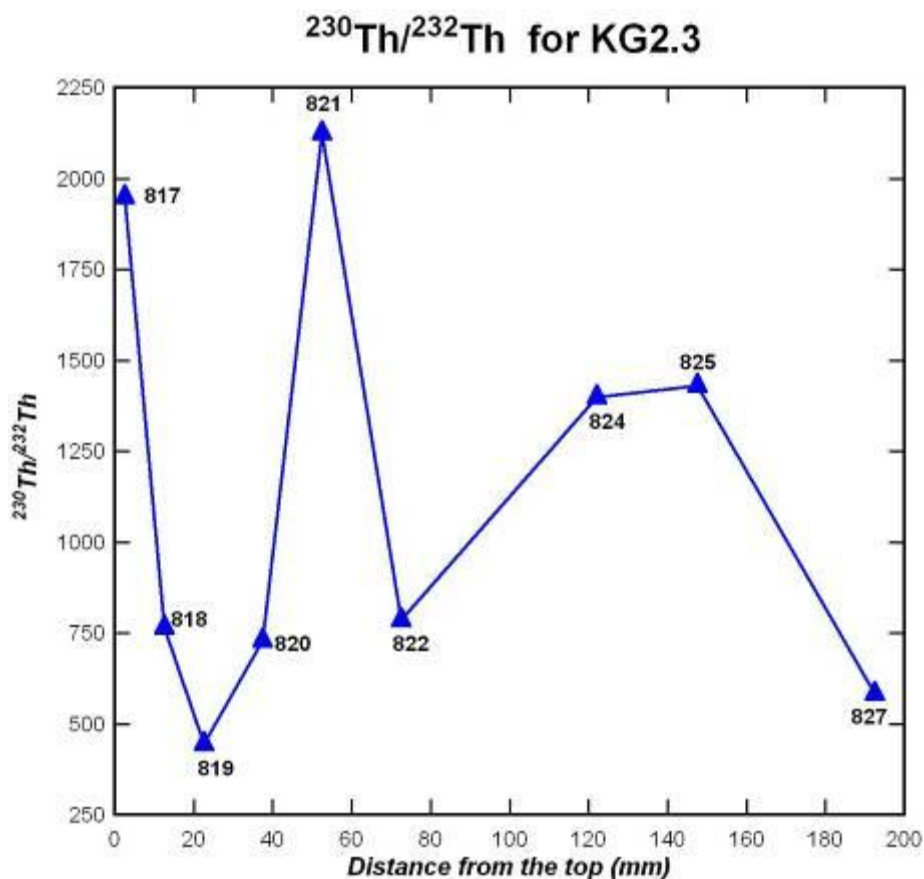


Figure 5.3 Variation in the KG2.3 $^{230}\text{Th}/^{232}\text{Th}$ activity ratios

Besides the influence of ^{230}Th contamination, uranium leaching may produce discrepancies between the U-series derived dates and the stratigraphy of a sample. Leaching may occur during speleothem formation and post-deposition. Possible leaching is identified from changes in the initial $^{234}\text{U}/^{238}\text{U}$ ratio that are in turn related to conditions in the ground water system from which carbonate is derived (e.g. Whitehead *et al.* 1999).

When ^{234}U is leached into the groundwater through the erosion of older host rocks excess U enters the percolation solution. Calcite formed from this U-rich solution will consequently have lower ^{238}U concentrations compared to ^{234}U . Concomitant with the excess ^{234}U is higher $^{234}\text{U}/^{238}\text{U}$ and $^{230}\text{Th}/^{234}\text{U}$ ratios since the introduced ^{234}U will decay over time to produce ^{230}Th . This change in the $^{230}\text{Th}/^{234}\text{U}$ ratio will result in a U-series derived age that is too young. Over time, the percolation water depletes the excess U in the host rock and the continuous loss of ^{234}U

decreases the $^{234}\text{U}/^{238}\text{U}$ and $^{230}\text{Th}/^{234}\text{U}$ ratios and lowers the sample U concentrations through time (Grün *et al.* 1999). As a result, the initial $^{234}\text{U}/^{238}\text{U}$ ratios will be higher in older layers compared to younger ones.

In the *KG2.3* sample, the initial $^{234}\text{U}/^{238}\text{U}$ values varying between 1.75 and 1.60 were comparatively higher than the measured $^{234}\text{U}/^{238}\text{U}$ activity ratios, which ranged between 1.54 and 1.43 (Fig. 5.4). This could reflect the depletion of excess ^{234}U in the overlying host rock or be related to a decline in available U taken up by the percolation water.

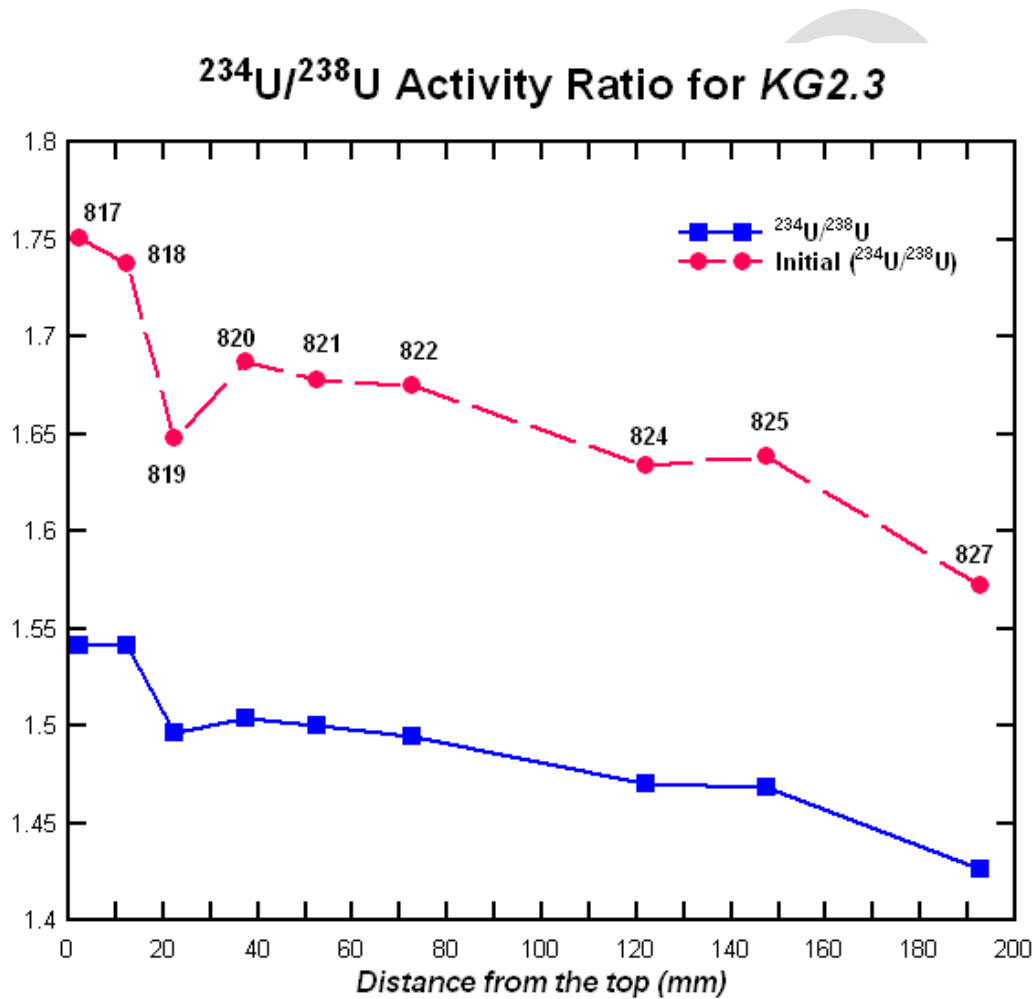


Figure 5.4 Plot of the $^{234}\text{U}/^{238}\text{U}$ and initial $^{234}\text{U}/^{238}\text{U}$ activity ratios for *KG2.3* and the corresponding sample lab numbers. The initial $^{234}\text{U}/^{238}\text{U}$ activity ratios are indicative of the geochemical conditions in the drip water at the time of calcite precipitation (which are related primarily the solubility of ^{234}U). Changes in the $^{234}\text{U}/^{238}\text{U}$ values therefore allow one to assess the extent to which the U system of the sample has been damaged by leaching of ^{234}U

The $^{230}\text{Th}/^{234}\text{U}$ ratios followed the trend observed with the $^{234}\text{U}/^{238}\text{U}$ activity ratios (Fig. 5.5). This decrease in $^{234}\text{U}/^{238}\text{U}$, $^{230}\text{Th}/^{234}\text{U}$ and ^{238}U (ppm) is broadly consistent with conditions of either continuous or partial leaching of ^{234}U (Grün *et al.* 1999).

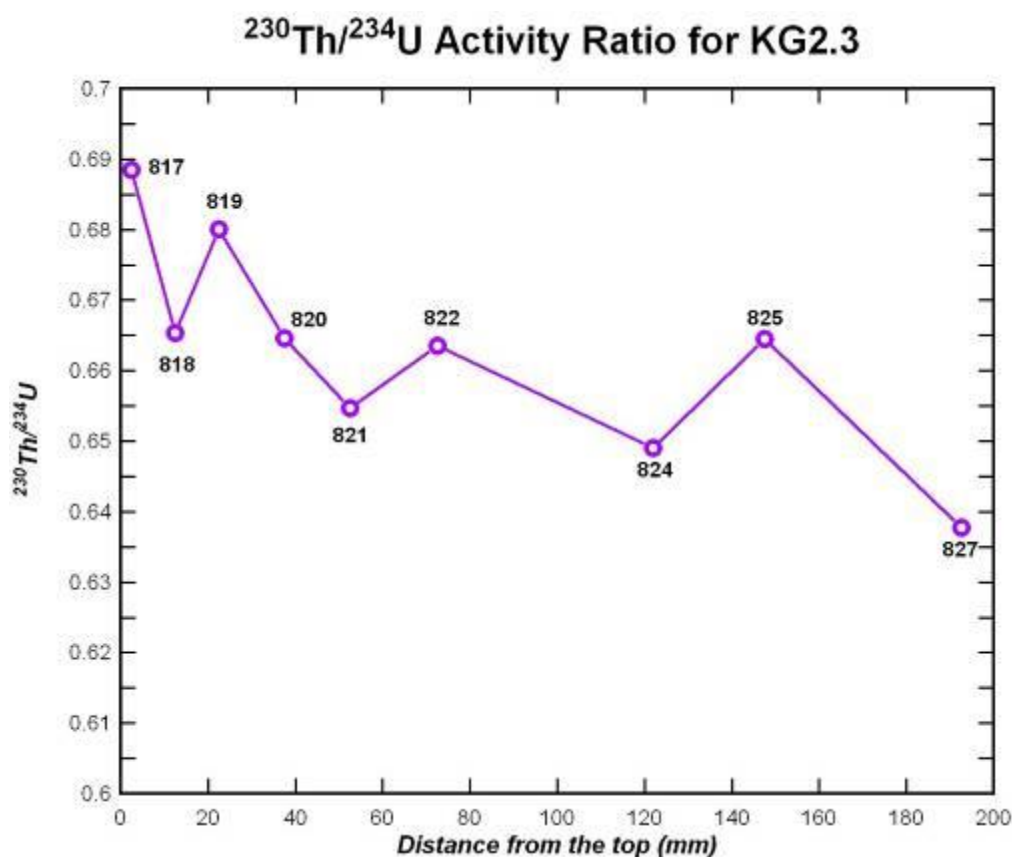


Figure 5.5 Activity ratio of $^{230}\text{Th}/^{234}\text{U}$ for KG2.3

On the other hand, all the KG2.3 activity ratios are within the range of variability observed in *Bloul*. The geochemical data consequently provides no clarity regarding the stratigraphic ambiguity observed in the KG2.3 sample.

Initially, the author thought that the KG2.3 stalagmite was upside down but this seems doubtful as growth bands in stalagmites typically bend down towards the sides. In KG2.3 these laminations have a wave-like appearance (see Chapter 4 Fig. 4.10 & *cf.* Fig. 4.7). It is possible that the subsamples were mixed up or mislabelled prior to the ICP MS analysis but this is highly unlikely. Machine discrepancies are also excluded as issues regarding the calibration of the Nu Plasma ICP MS were resolved by the time the KG2.3 samples were run.

The exact cause of the stratigraphic discrepancies observed in *KG2.3* is presently unknown. It is noteworthy that similar ambiguities were observed in the *KG2.2* flowstone sample from Kaisers Gat II. For this reason it is suggested that the differences observed in the *KG2.3* stalagmite and the *KG2.2* flowstone were possibly caused by factors related to the conditions inside the cave.

Based on the available data it appears that all the U-series ages for *KG2.3* fall within MIS 5c/d. Although annual laminations may be present in this sample, it is proposed that the stalagmite possibly formed quite rapidly from *c.* 103 - *c.* 115 ka. Since the corresponding stable isotope values are likely to reflect the general environmental conditions in the vicinity of the cave during the interval represented by the *KG2.3* record, average $\delta^{13}\text{C}$ and $\delta^{18}\text{O}$ values may be used for palaeoenvironmental interpretations (see section 5.2.2).

KG2.2 sample

Similar disagreements between the U-series derived age and the stratigraphy were observed in *KG2.2* (see Table 6.3). In this sample (*i.e.* *KG2.2*) however Th contamination was particularly high in the subsamples taken from the top (0-9 mm) and bottom (46-52 mm) of the flowstone (Table 5.2). Since Th contamination greatly reduces the reliability of the U-series age these samples were not considered for the age-depth model (section 5.2.3).

Blou1 sample

Stalagmite growth in the *Blou1* sample occurred *c.* 48 ka with good agreement between the growth laminations and the U-series age estimates (Fig. 5.6). Two distinct growth intervals were identified for this stalagmite. The first growth phase occurred during the late Holocene *c.* 3.5 ka. At this stage, the upper section (0 -18 mm) of the *Blou1* stalagmite comprises aragonite. Because the region immediately above the hiatus was not dated, the growth for the aragonite section of the sample could not be determined (Fig. 5.6). For comparative purposes, however, it is hypothesised that the isotopic values corresponding to the upper section of the stalagmite could be of late Holocene age.

The second phase of active growth occurred at a rate of $0.0183 \mu\text{m}/\text{year}$ from *c.* 45-47.8 ka. No visible signs of hiatus were observed in the growth laminations coinciding with this period although short intervals of discontinuous deposition may well exist. Between 45 ka and the late Holocene at *c.* 3.5 ka, there appears to have been a hiatus in stalagmite formation. The hiatus was recognised from the large gap between dates obtained from closely spaced subsamples (Fig. 5.6).

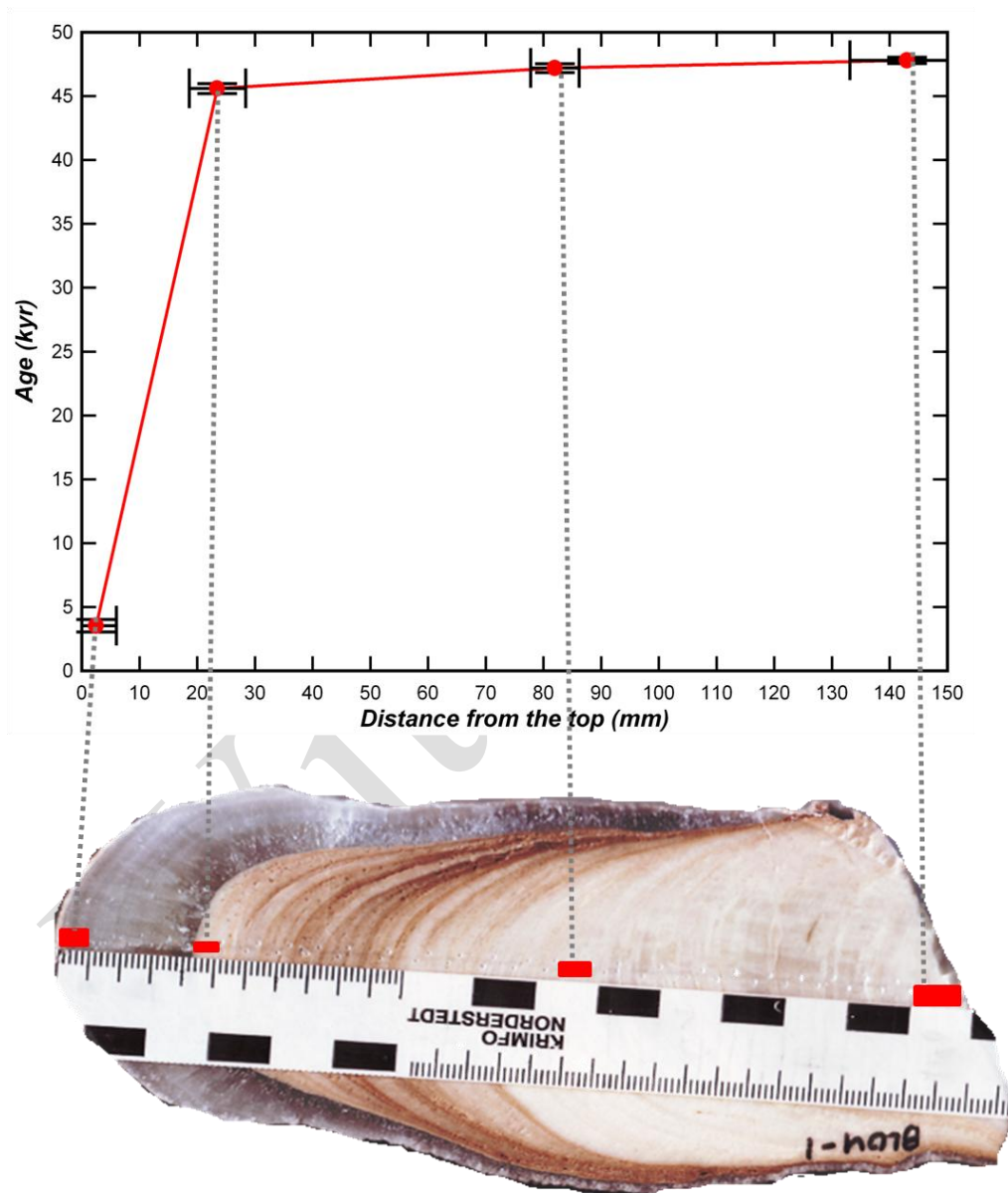


Figure 5.6 An age-stratigraphic plot for sample *Blou1* from Bloukrantz Cave. The U-series sample locations are represented by red blocks

5.2 Stable isotope signals

As outlined in section 4.6 of Chapter 4, variations in the oxygen isotope ratios are mainly affected by rainfall seasonality and temperature (*e.g.* Bar-Matthews *et al.* 1996; Harmon *et al.* 2004). The $\delta^{18}\text{O}$ signal is generally used for inferences of palaeotemperatures and changes in precipitation (*e.g.* Cruz Jr. *et al.* 2005; Johnson *et al.* 2006). Variations in the carbon isotope ratio by contrast are strongly influenced by the photosynthetic pathway used by the dominant vegetation in an area.

The stable isotope data recorded from the De Hoop speleothems is presented in Table 5.4.

Table 5.4 Summary of the $\delta^{13}\text{C}$ and $\delta^{18}\text{O}$ data obtained on the *Blou1*, *KG2.1*, *KG2.2* and *KG2.3* samples. The stable isotope values are reported relative to V-PDB

Cave	Lab No.	Sample Id.	Sample (mm)	Sample (μg)	$\delta^{13}\text{C}$ (‰)	$\delta^{18}\text{O}$ (‰)
BLOU	43	JN43	1	90	-3.15	-3.09
BLOU	153	JN153	2	123	-3.05	-3.05
BLOU	44	JN44	4	90	-4.32	-3.58
BLOU	154	JN154	4	64	-5.33	-4.10
BLOU	155	JN155	6	65	-4.89	-3.96
BLOU	45	JN45	7	100	-6.09	-3.87
BLOU	46	JN46	8	100	-6.63	-4.40
BLOU	156	JN156	9	63	-5.74	-4.06
BLOU	47	JN47	11	100	-7.40	-4.60
BLOU	48	JN48	13	100	-7.57	-4.52
BLOU	157	JN157	13	111	-7.88	-4.71
BLOU	160	JN160	15	111	-8.42	-4.87
BLOU	49	JN49	16	100	-7.63	-4.44
BLOU	158	JN158	17	80	-7.02	-4.06
BLOU	50	JN50	18	90	-7.93	-4.45
BLOU	159	JN159	19	88	-6.87	-4.37
BLOU	51	JN51	21	90	-7.38	-4.77
BLOU	52	JN52	21	90	-7.52	-4.86
BLOU	161	JN161	22	90	-4.67	-2.75
BLOU	162	JN162	24	90	-3.85	-2.57
BLOU	53	JN53	25	100	-4.68	-2.64
BLOU	54	JN54	26	90	-4.98	-2.70
BLOU	163	JN163	27	90	-5.09	-2.81
BLOU	164	JN164	28	90	-5.42	-2.91
BLOU	55	JN55	30	100	-5.79	-2.82
BLOU	165	JN165	33	100	-2.37	-1.83
BLOU	166	JN166	34	100	-2.51	-1.84
BLOU	57	JN57	35	100	-3.49	-2.08
BLOU	58	JN58	37	100	-3.32	-2.22
BLOU	59	JN59	40	90	-3.19	-2.12

BLOU	60	JN60	41	90	-4.50	-2.62
BLOU	167	JN167	42	90	-1.47	-1.44
BLOU	168	JN168	44	90	-1.92	-1.61
BLOU	61	JN61	45	90	-2.11	-1.71
BLOU	62	JN62	46	100	-1.16	-1.38
BLOU	169	JN169	47	100	-1.76	-1.70
BLOU	170	JN170	48	100	-1.16	-1.36
BLOU	171	JN171	50	100	-2.10	-1.80
BLOU	63	JN63	51	90	-1.46	-1.50
BLOU	64	JN64	52	100	-2.30	-1.58
BLOU	172	JN172	55	100	-2.47	-1.87
BLOU	65	JN65	56	90	-2.05	-1.67
BLOU	173	JN173	57	90	-2.73	-2.10
BLOU	66	JN66	58	90	-2.47	-1.83
BLOU	174	JN174	59	90	-3.13	-2.02
BLOU	175	JN175	59	90	-3.07	-1.97
BLOU	67	JN67	61	90	-3.58	-2.13
BLOU	176	JN176	61	90	-2.54	-1.74
BLOU	68	JN68	63	90	-2.79	-1.77
BLOU	177	JN177	63	90	-2.10	-1.67
BLOU	69	JN69	66	90	-2.59	-1.79
BLOU	70	JN70	68	90	-2.31	-1.68
BLOU	71	JN71	72	100	-2.86	-2.09
BLOU	72	JN72	73	90	-2.21	-1.64
BLOU	179	JN179	73	90	-2.48	-2.29
BLOU	178	JN178	74	90	-3.39	-1.91
BLOU	73	JN73	77	90	-2.70	-1.81
BLOU	74	JN74	78	90	-2.88	-1.94
BLOU	180	JN180	78	90	-2.79	-1.97
BLOU	75	JN75	81	90	-3.42	-2.06
BLOU	76	JN76	83	90	-3.37	-2.07
BLOU	181	JN181	84	90	-3.08	-2.03
BLOU	77	JN77	86	90	-3.26	-2.04
BLOU	78	JN78	88	100	-2.98	-2.02
BLOU	182	JN182	90	100	-2.96	-2.13
BLOU	79	JN79	92	90	-2.76	-1.97
BLOU	183	JN183	94	90	-3.63	-2.14
BLOU	80	JN80	95	90	-3.04	-2.12
BLOU	184	JN184	97	90	-2.92	-1.94
BLOU	81	JN81	100	100	-4.46	-2.33
BLOU	82	JN82	102	100	-4.13	-2.24

BLOU	83	JN83	105	100	-4.43	-2.19
BLOU	185	JN185	106	100	-3.49	-2.35
BLOU	84	JN84	107	90	-5.05	-2.54
BLOU	85	JN85	110	90	-3.35	-1.97
BLOU	86	JN86	112	100	-4.21	-2.53
BLOU	186	JN186	112	100	-2.70	-2.72
BLOU	87	JN87	115	100	-3.06	-1.92
BLOU	88	JN88	117	90	-3.16	-1.97
BLOU	89	JN89	120	100	-3.25	-2.04
BLOU	90	JN90	123	90	-3.92	-2.31
BLOU	187	JN187	123	90	-3.24	-2.34
BLOU	188	JN188	123	90	-4.73	-2.65
BLOU	91	JN91	125	100	-4.81	-2.59
BLOU	92	JN92	128	90	-3.03	-1.96
BLOU	189	JN189	128	90	-4.27	-2.22
BLOU	93	JN93	130	100	-4.38	-2.30
BLOU	94	JN94	132	90	-5.17	-2.69
BLOU	95	JN95	135	90	-5.20	-2.59
BLOU	96	JN96	137	90	-4.40	-2.34
BLOU	190	JN190	138	90	-3.16	-1.32
BLOU	97	JN97	140	90	-3.87	-2.16
BLOU	98	JN98	141.5	90	-4.35	-2.29
KG2.1	1	JN01	7	51	-5.54	-3.23
KG2.1	131	JN131	9	51	-8.12	-4.02
KG2.1	132	JN132	11	51	-8.49	-4.01
KG2.1	2	JN02	12	51	-7.00	-3.43
KG2.1	133	JN133	12	51	-8.06	-4.01
KG2.1	134	JN134	13	51	-8.18	-4.42
KG2.1	135	JN135	14	51	-7.98	-4.08
KG2.1	136	JN136	15	51	-8.40	-3.97
KG2.1	137	JN137	16	51	-8.72	-4.18
KG2.1	3	JN03	17	51	-8.28	-4.17
KG2.1	138	JN138	17	51	-9.11	-4.18
KG2.1	139	JN139	18	51	-9.35	-3.63
KG2.1	140	JN140	19	51	-9.33	-3.54
KG2.1	141	JN141	20	51	-7.42	-3.77
KG2.1	142	JN142	22	51	-7.59	-3.95
KG2.1	143	JN143	23	51	-5.78	-3.35
KG2.1	144	JN144	24	51	-6.00	-3.75
KG2.1	4	JN04	25	51	-5.22	-2.89
KG2.1	145	JN145	26	51	-7.52	-3.61

KG2.1	146	JN146	28	51	-7.44	-3.93
KG2.1	147	JN147	29	51	-7.54	-5.60
KG2.1	149	JN149	32	51	-6.55	-3.37
KG2.1	150	JN150	34	51	-5.51	-3.17
KG2.1	151	JN151	35	51	-7.12	-3.54
KG2.1	152	JN152	36	51	-6.41	-3.57
KG2.2	100	JN100	2	90	-6.71	-3.89
KG2.2	101	JN101	6	90	-7.67	-3.71
KG2.2	102	JN102	8	90	-7.87	-3.75
KG2.2	116	JN116	9	90	-7.91	-3.76
KG2.2	118	JN118	11	90	-6.41	-3.49
KG2.2	103	JN103	11.5	90	-5.95	-2.98
KG2.2	104	JN104	13.5	90	-7.73	-3.90
KG2.2	106	JN106	16	100	-7.54	-3.80
KG2.2	119	JN119	16	100	-6.96	-4.02
KG2.2	105	JN105	18	100	-6.85	-4.02
KG2.2	108	JN108	21	90	-6.53	-3.43
KG2.2	120	JN120	21	90	-5.10	-3.43
KG2.2	107	JN107	23	90	-6.32	-3.53
KG2.2	110	JN110	25	90	-7.10	-3.77
KG2.2	109	JN109	27	90	-7.06	-3.86
KG2.2	121	JN121	30	90	-5.54	-3.15
KG2.2	111	JN111	31	90	-7.32	-3.84
KG2.2	122	JN122	31	90	-6.90	-3.65
KG2.2	112	JN112	34	100	-6.90	-3.15
KG2.2	123	JN123	34	100	-7.25	-3.37
KG2.2	113	JN113	38	100	-7.51	-3.80
KG2.2	124	JN124	38	100	-6.57	-3.36
KG2.2	114	JN114	41	90	-7.06	-3.20
KG2.2	115	JN115	44	90	-5.49	-3.40
KG2.2	125	JN125	44	90	-6.94	-3.46
KG2.3	41	JN41	2	100	-9.95	-2.94
KG2.3	42	JN42	5	100	-10.30	-2.99
KG2.3	40	JN40	7	100	-6.85	-1.35
KG2.3	39	JN39	10	110	-9.39	-2.44
KG2.3	6	JN06	14	90	-9.21	-2.56
KG2.3	5	JN05	15	100	-8.95	-2.26
KG2.3	8	JN08	28	110	-8.19	-1.51
KG2.3	7	JN07	30	120	-8.45	-2.10
KG2.3	9	JN09	44	120	-9.24	-2.06
KG2.3	10	JN10	46	100	-8.47	-2.16

KG2.3	12	JN12	61	100	-9.37	-2.60
KG2.3	14	JN14	73	90	-10.40	-3.26
KG2.3	13	JN13	75	110	-10.68	-3.56
KG2.3	16	JN16	88	100	-9.36	-2.75
KG2.3	15	JN15	90	110	-9.09	-2.38
KG2.3	18	JN18	103	120	-9.81	-3.03
KG2.3	17	JN17	105	120	-10.07	-2.51
KG2.3	20	JN20	117	110	-9.32	-2.53
KG2.3	19	JN19	120	100	-9.74	-3.42
KG2.3	22	JN22	132	110	-9.03	-2.40
KG2.3	21	JN21	135	110	-8.10	-2.09
KG2.3	24	JN24	147	100	-9.25	-2.44
KG2.3	23	JN23	150	90	-9.45	-2.70
KG2.3	26	JN26	161	90	-3.31	0.51
KG2.3	25	JN25	165	100	-9.78	-3.14
KG2.3	28	JN28	176	90	-9.17	-2.46
KG2.3	27	JN27	180	100	-8.74	-2.55
KG2.3	30	JN30	183	110	-9.05	-2.91
KG2.3	29	JN29	185	120	-8.60	-2.39
KG2.3	32	JN32	188	120	-7.52	-2.03
KG2.3	31	JN31	190	120	-9.09	-2.96
KG2.3	33	JN33	194	120	-8.31	-2.85
KG2.3	34	JN34	196	110	-8.14	-2.29
KG2.3	35	JN35	199	110	-9.20	-3.24
KG2.3	36	JN36	201	100	-9.43	-3.25
KG2.3	37	JN37	205	110	-10.46	-3.65
KG2.3	38	JN38	208	120	-8.80	-1.75

5.2.1 Evaluating kinetic fractionation & conditions of isotopic equilibrium

Relating the isotopic composition of the speleothems to specific environmental variables is however quite complex as a number of factors operating at local, regional and temporal scales can alter the drip water ^{13}C and ^{18}O composition (*e.g.* Bar-Matthews *et al.* 1996; Baker *et al.* 1997; Baldini *et al.* 2005, 2006; Mickler *et al.* 2006). In addition, fractionation effects (*viz.* evaporation) which are not necessarily climatically determined but are operating within the cave environment may also cause variations in the carbon and oxygen isotopic signature.

With regard to $\delta^{13}\text{C}$, the composition of the host rock, the time it takes for the percolation solution to enter the cave and the dominant vegetation overlying the cave can influence the isotopic signal. The latter effect is determined primarily from the photosynthetic pathway of the vegetation and is considered the most significant contributor to the drip water $\delta^{13}\text{C}$. Most notably kinetic fractionation effects related to evaporation and temperature changes affect the $\delta^{18}\text{O}$ signal. Evaporative changes are related to the hydrological cycle whereas temperature dependent variations are linked to calcite precipitation. The latter effect is influenced by the fractionation between the speleothem calcite and the drip water solution (see Chapter 4). Identifying kinetic fractionation effects is particularly important as fractionation related shifts in the isotopic signal could often produce ambiguous values. This consequently makes palaeoenvironmental interpretations more difficult.

It is therefore necessary to determine the extent to which the isotope values are truly indicative of changing environmental conditions above the cave. Hendy (1971) developed the first test to do this. This test is named the Hendy Test and is based on the concept of isotopic equilibrium. The Hendy Test characterises isotopic equilibrium by the following factors:

1. slow degassing rates (*c.* 2×10^3 s)
2. negligible evaporation
3. constant $\delta^{18}\text{O}$ values along a single growth layer
4. no relationship between the $\delta^{18}\text{O}$ and $\delta^{13}\text{C}$ isotopic values

Based on criterion 3 and 4, non-equilibrium deposition or kinetic fractionation effects are identified when there is a linear correlation between $\delta^{18}\text{O}$ and $\delta^{13}\text{C}$ isotopic values. The premise for this correlation is that if evaporative effects are significant then both $\delta^{18}\text{O}$ and $\delta^{13}\text{C}$ become progressively enriched along a growth layer (Lauritzen & Lundberg 1999).

From the covariation observed between the $\delta^{18}\text{O}$ and $\delta^{13}\text{C}$ values recorded for both *Blou1* and *KG2.3* it appears that these speleothems may have formed out of

isotopic equilibrium (Figs 5.7a, b). The isotopic values from the *Blou1* sample were only taken from the calcite portion and did not include the isotope values corresponding to the hiatus.

Although the Hendy Test is commonly used, it is not always considered an accurate means for identifying equilibrium deposition (*e.g.* Lauritzen & Lundberg 1999; Dorale *et al.* 2002; Lachniet 2009). The replication test, proposed by Dorale *et al.* (2002) is considered a strong and cogent indicator of deposition under equilibrium conditions. This replication test is based on congruent $\delta^{13}\text{C}$ and $\delta^{18}\text{O}$ profiles obtained from similar aged speleothems sampled from the same or nearby caves (*e.g.* Dorale & Lui 2009). Equilibrium conditions are then implied by similarities in the isotope ratios obtained from these samples even if they may have formed under non-equilibrium conditions. As a result, congruence in isotopic profiles between nearby sites are more likely to reflect regional climatic controls rather than variations in the local hydrology or degassing rates (*e.g.* Baker *et al.* 1996; Dorale *et al.* 1998; Constantin *et al.* 2007).

Therefore although the Hendy Test indicated that the De Hoop speleothem samples were possibly unsuitable for palaeoenvironmental interpretations, the replication approach was used as an alternative.

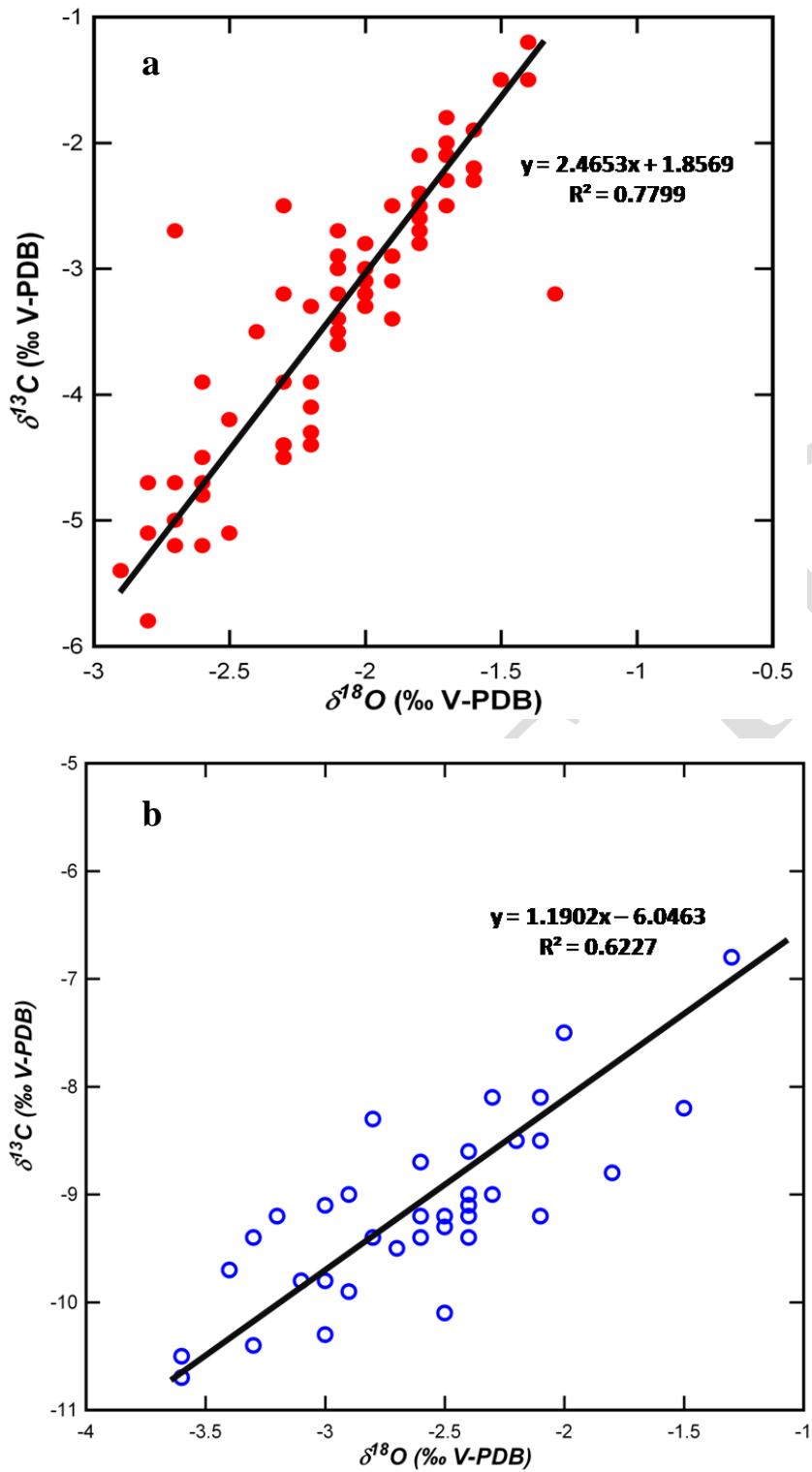


Figure 5.7 (a) Hendy Test applied to the Bloukrantz Cave (*Blou1*) and (b) Kaisers Gat II (*KG2.3*) speleothems. The *Blou1* data is represented by the closed (red) dots. The open (blue) dots represent the *KG2.3* values

With regard to the *Blou1* stalagmite, the isotopic profile of this sample was compared to the one obtained from the *KG2.2*. The latter sample was obtained from Kaisers Gat II, which is *c.* 8 km from Bloukrantz Cave where the *Blou1* sample was taken. The *Blou1* sample is dated from 3.5 to 50 ka and the age estimates for the *KG2.2* sample are *c.* 49 and 41 ka (see Table 5.3). Although the *KG2.2* sample contains fewer isotope subsamples than *Blou1*, the overlap in the $\delta^{13}\text{C}$ and $\delta^{18}\text{O}$ values from these samples suggests that the isotopic profile of *Blou1* could have been determined by a climatic influence and not necessarily kinetic fractionation effects (Fig. 5.8). Unfortunately, since the *KG2.2* ages are stratigraphically inverted it is possible that the *Blou1* and *KG2.2* samples may not be contemporaneous.

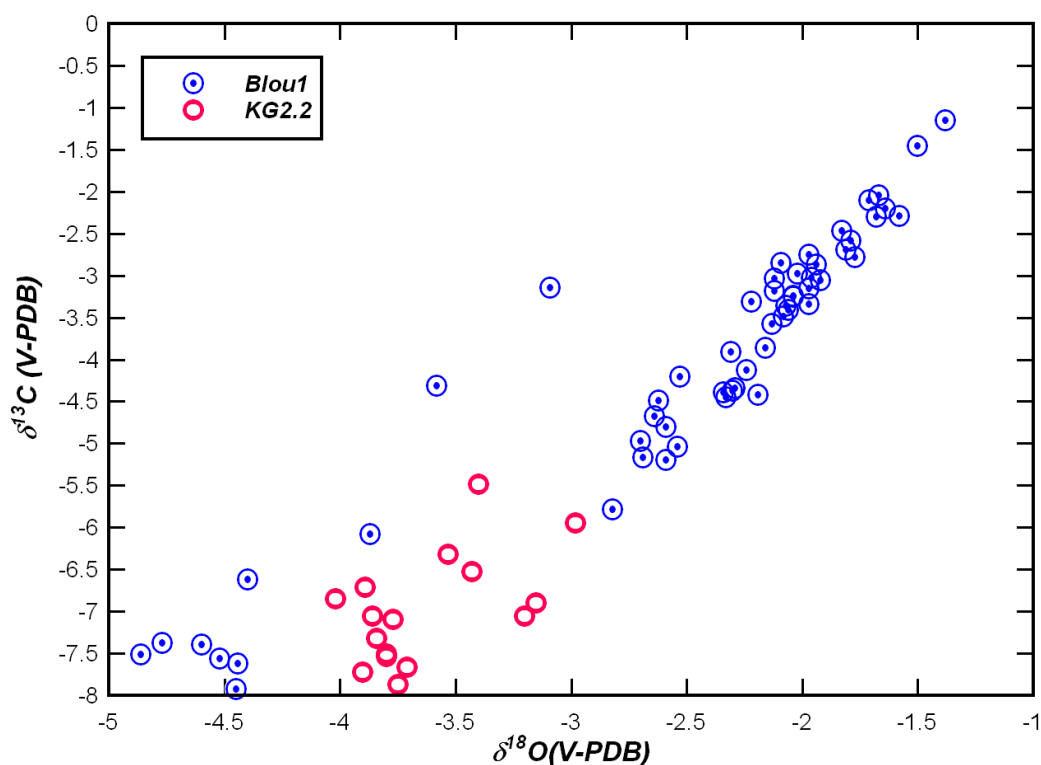


Figure 5.8 Comparison of the stable carbon and oxygen isotope signals preserved in the speleothems from the Bloukrantz Cave (*Blou1*) and Kaisers Gat II (*KG2.2*)

The replication test could not be applied to the *KG2.3* stalagmite since there were no suitably dated speleothems within the 100 kyr range of this sample.

Comparisons between the *KG2.3* isotope curves with the speleothem record from

Crevice Cave as well as related palaeoenvironmental contexts will serve as a replication test *sensu lato*. Similarities with other dated records will add credence to the palaeoenvironmental interpretations based on the *KG2.3* stalagmite record.

5.2.2 $\delta^{13}\text{C}$ and $\delta^{18}\text{O}$ profile of the individual samples

In *Blou1*, the $\delta^{13}\text{C}$ values vary between -8.4 and -1.1 ‰ and the $\delta^{18}\text{O}$ values range from -4.8 and -1.3 ‰ with mean isotopic values of -3.9 ‰ for $\delta^{13}\text{C}$ and -2.5 ‰ for $\delta^{18}\text{O}$. A local peak in both the $\delta^{13}\text{C}$ and $\delta^{18}\text{O}$ values is coeval with the termination of the depositional hiatus; $\delta^{13}\text{C}$ values increased from -7.4 ‰ to -3.2 ‰ at the top of the stalagmite while $\delta^{18}\text{O}$ values changed from -3.1 to -4.9 ‰. This interval coincides with the deposition of aragonite in the *Blou1* stalagmite. A second period of isotopic fluctuation falls between 45 and 143 mm (Fig. 5.9). During this stage, $\delta^{13}\text{C}$ and $\delta^{18}\text{O}$ are more positive (*i.e.* enriched or higher) with values between -4.5 and -1.0 ‰ for ^{13}C and -2.6 and -1.5 ‰ for ^{18}O .

Bloukrantz Cave (Blou1)

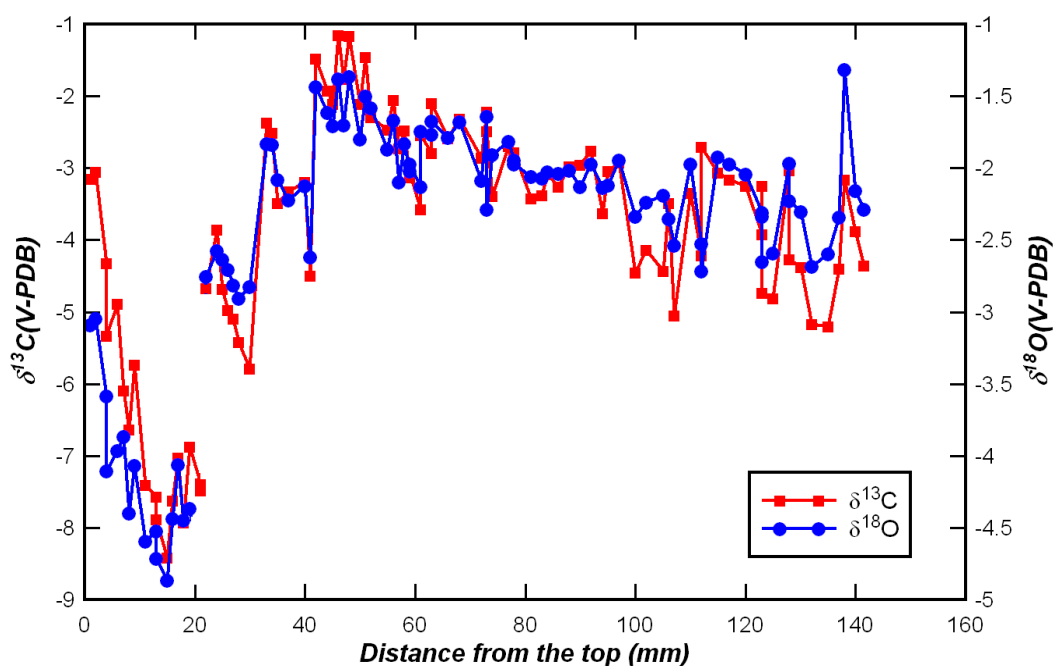


Figure 5.9 Variations in $\delta^{13}\text{C}$ and $\delta^{18}\text{O}$ sampled from the *Blou1* stalagmite

In the *KG2.1* stalagmite $\delta^{13}\text{C}$ values ranged from -9.3 and -5.2 ‰ with a mean of -7.4 ‰. The $\delta^{18}\text{O}$ varied between -5.6 and -2.9 ‰ with an average value of -3.8 ‰.

Peaks and dips in the $\delta^{13}\text{C}$ were mirrored by corresponding shifts in $\delta^{18}\text{O}$ values. This trend was noted in the first 25 mm sampled from the top of the stalagmite. Between 25 and 30 mm there was a slight lag between $\delta^{13}\text{C}$ and $\delta^{18}\text{O}$; at 29 mm for example, $\delta^{18}\text{O}$ values changed sharply from enriched in ^{18}O at -3.9 ‰ to depleted in the heavier ^{18}O isotope at -5.6 ‰. The magnitude of change in $\delta^{13}\text{C}$ by contrast was quite small (c. -0.1 ‰). Both $\delta^{13}\text{C}$ and $\delta^{18}\text{O}$ peak again at 35 mm with isotopic values of -7.1 ‰ and -3.5 ‰, respectively (Fig. 5.10).

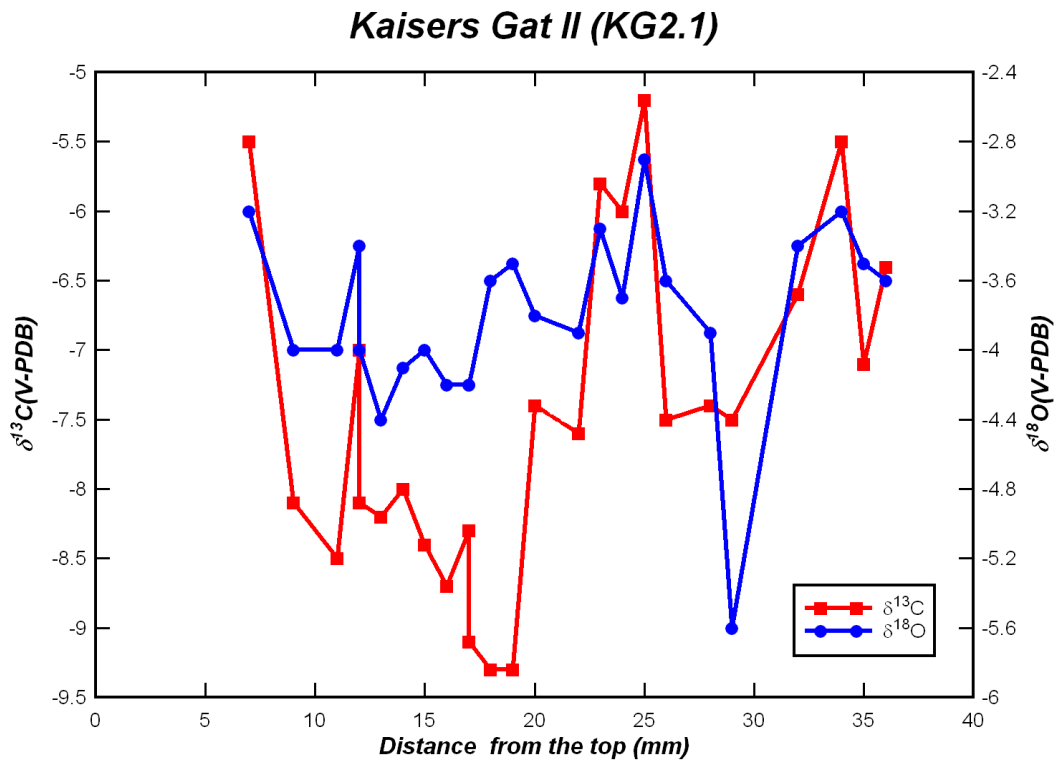


Figure 5.10 Variations in the $\delta^{13}\text{C}$ and $\delta^{18}\text{O}$ isotopic profile of the *KG2.1* stalagmite

In sample *KG2.2* $\delta^{13}\text{C}$ values ranged from -7.9 to -5.9 ‰ and the $\delta^{18}\text{O}$ varied between -4.0 and -3.0 ‰. Isotopic values fluctuate throughout the sequence with peaks in $\delta^{13}\text{C}$ values occurring at 11 mm (-6.4 ‰), 21 mm (-6.5 ‰), 30 mm (-5.5 ‰) and 44 mm (-5.5 ‰). The $\delta^{18}\text{O}$ signal followed a similar trend to the $\delta^{13}\text{C}$ profile however the amplitude of the $\delta^{18}\text{O}$ peaks is much smaller (Fig. 5.11). Overall, this sample exhibited mean isotopic values of -6.8 ‰ for $\delta^{13}\text{C}$ and -3.5 ‰ for $\delta^{18}\text{O}$ relative to V-PDB (Fig. 5.11).

Kaisers Gat II (KG2.2)

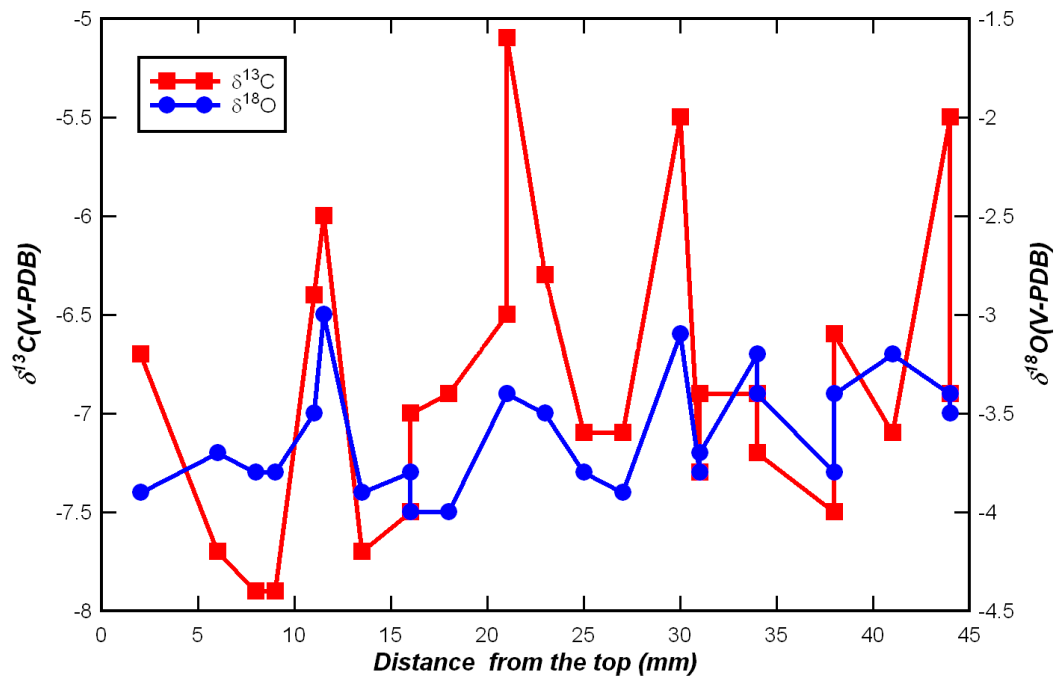


Figure 5.11 $\delta^{13}\text{C}$ and $\delta^{18}\text{O}$ values obtained from the KG2.2 flowstone

The $\delta^{13}\text{C}$ values for KG2.3 range from -10.7 to -6.8 ‰ and the $\delta^{18}\text{O}$ values vary between -1.34 and -3.64 ‰. The $\delta^{13}\text{C}$ and $\delta^{18}\text{O}$ values co-vary down the length of the stalagmite with peaks and dips in the isotopic values recorded throughout. An average $\delta^{13}\text{C}$ value of -9.1 ‰ and a $\delta^{18}\text{O}$ value of -2.6 ‰ were recorded for KG2.3 (Fig. 5.12). As mentioned previously, deviations from these mean values will be used for further interpretations.

Kaisers Gat II (KG2.3)

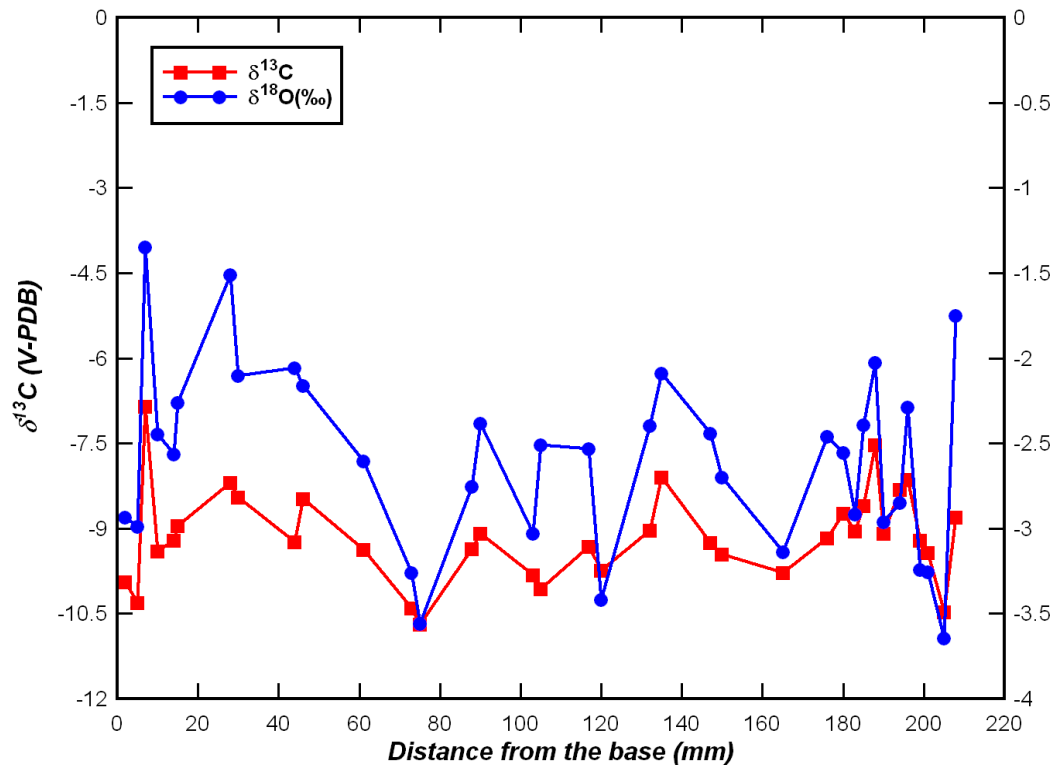


Figure 5.12 $\delta^{13}\text{C}$ and $\delta^{18}\text{O}$ data for the KG2.3 stalagmite

5.2.3 Isotope age calibration curve

An isotope based age chronology was established for the speleothem samples in order to evaluate inter-sample comparisons and for comparing the De Hoop isotope curves with other proxy records. The model was created using a linear regression over sections of constant growth rate. The ages were then interpolated stratigraphically within each of the U-series dated points as follows:

Firstly, a straight line in the form of $y = ax + b$ was calculated between the first two points and used to estimate the ages of the corresponding isotope values within the interval described by the line. Similarly, a second line was determined for the remaining two points. This is illustrated using the *Blou1* curve (Fig. 5.13). The slope of the line (*i.e.* the growth rate) is represented by (a) whereas (b) refers to the intercept. The x corresponds to the distance (mm) and the age (ka) is described by the y value.

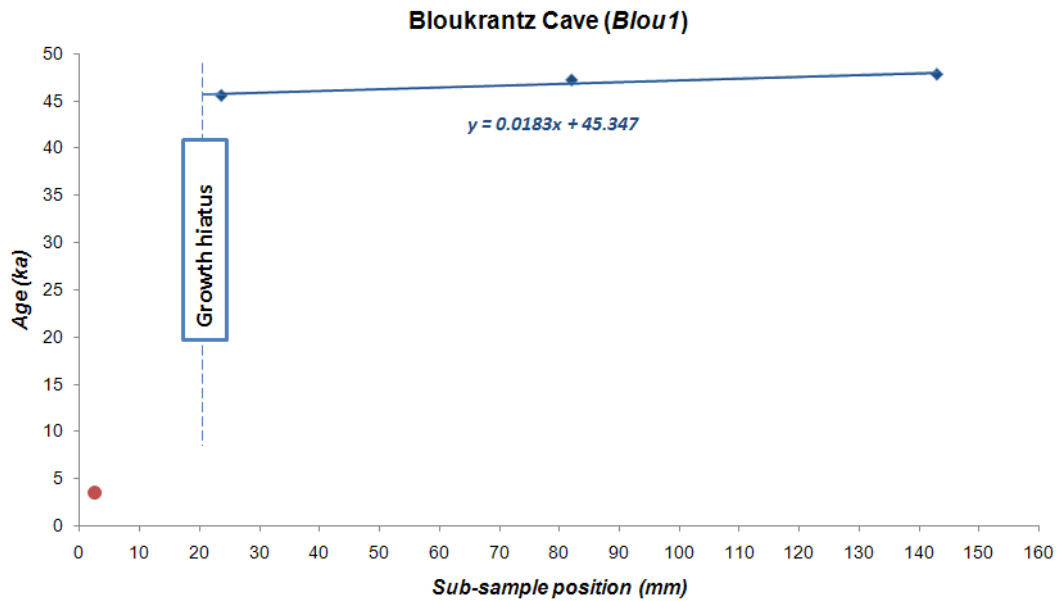


Figure 5.13 Trend line representing the main growth phase in the development of the *Blou1* stalagmite. This phase is described by $y = 0.0183x + 44.54$. This plot is based on the tabulated U-series ages. The growth rate expressed in units of mm/ka is determined from the slope of the line

Since each of the points specified by the line comprises a distance (x-value) and age (y-value) component, these points are renamed as x_1, y_1 and x_2, y_2 . The slope of the line a (which describes the growth rate) between the two points is therefore

$$(y_2 - y_1)/(x_2 - x_1)$$

Given that the interpolation uses a straight line between two known values to estimate a new value, all successive x-values are subtracted from x_1 . For the corresponding y-values, y_1 (or the next U-series dated point) is added to each value.

The equation for each of the interpolated points between the two dated zones is therefore described mathematically as:

$$y = (x - x_1) \times [(y_2 - y_1)/(x_2 - x_1)] + y_1$$

In this equation x is the new position between the two points. The above expression was also used to extrapolate the ages beyond the range of the *Blou1* profile. A similar approach was used to calculate the associated error intervals for the distance (mm) and age (ka) values.

Blou1 Age model curve

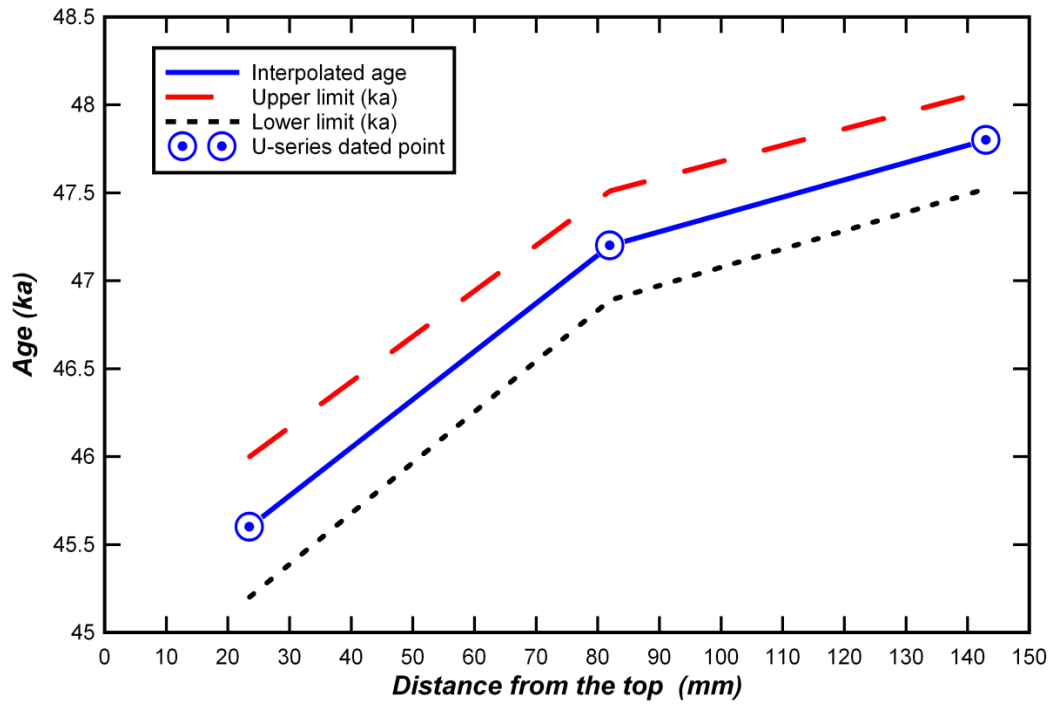


Figure 5.14 Age estimations based on the *Blou1* U-series dates and constructed using a linear interpolation formula. The central line represents the average age estimate. The other two lines denote, respectively, the upper and lower boundary of the interpolated ages. The actual U series dated position are represented by the \odot symbol

The interpolated ages and corresponding subsample positions were then used to generate a plot expressing the stable isotope points as an age (Fig. 5.15).

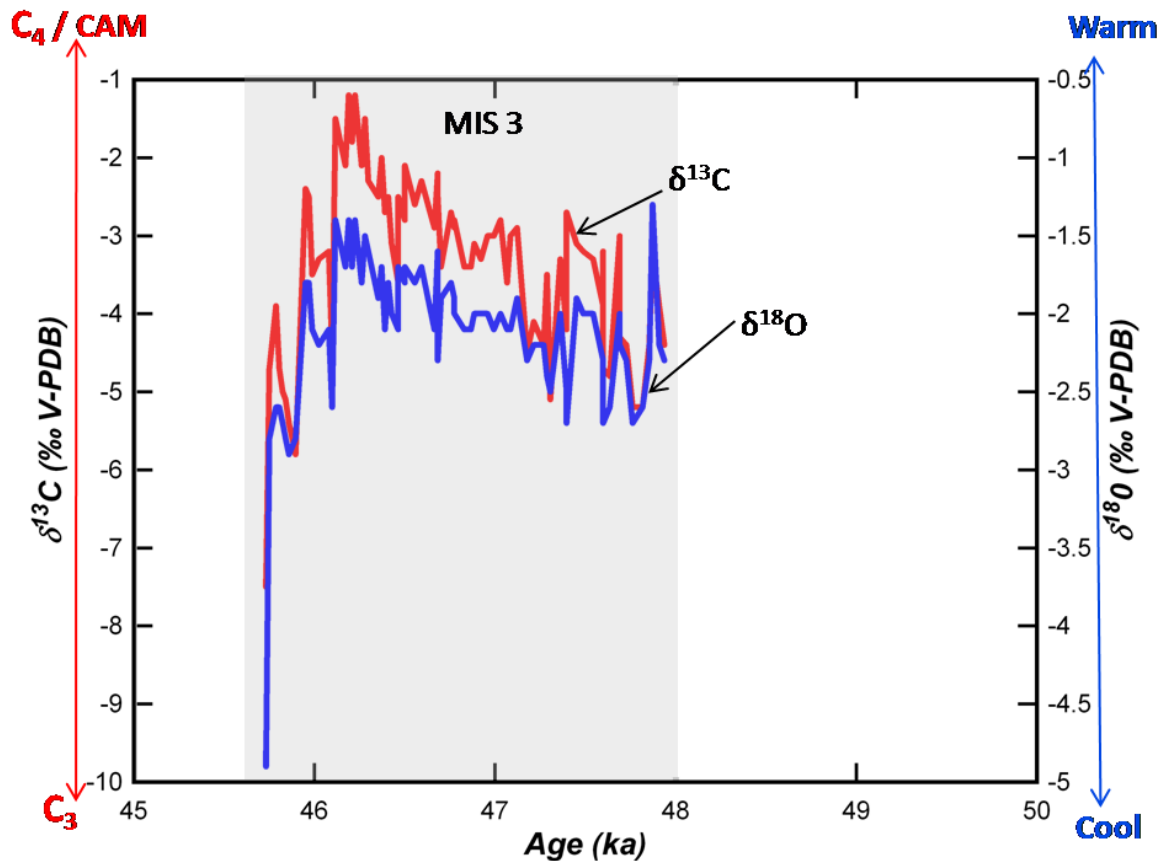


Figure 5.15 Isotope time-series curve for *Blou1* corresponding to MIS 3

5.3 Discussion of the *Blou1* and *KG2.3* isotope results

The $\delta^{13}\text{C}$ signal is affected, amongst others, by variations in the drip rate and percolation path, the isotopic composition of the host rock and soil conditions above the cave. The $\delta^{18}\text{O}$ profile is also associated with a number of complex factors, most notably rainfall seasonality and temperature. Chapter 4 provided an overview of the complexities associated with the use of these isotopes for palaeoenvironmental interpretations.

As a palaeoproxy, the speleothem $\delta^{13}\text{C}$ signal is generally indicative of the vegetation overlying the cave. The photosynthetic pathway used by the dominant plants, *viz.* C_3 and C_4 types determines the palaeovegetation signature. In a purely C_3 environment the speleothem calcite $\delta^{13}\text{C}$ signal is approximately -12.8‰ (V-PDB) and in a C_4

dominated environment the $\delta^{13}\text{C}_{\text{calcite}}$ is c. +1.2 ‰ (V-PDB) (Talma & Vogel 1992). The broad trend is that C_3 plants are ubiquitous in areas with summer aridity and winter rainfall whereas C_4 plants are more prevalent in summer rainfall regions.

In the year-round rainfall region of the southern Cape the extant vegetation comprises both C_3 and C_4 photosynthesising forms. The main C_3 plants are the fynbos and Afromontane forest. Fynbos is shrub-like, fire-adapted mosaic vegetation that is characterised by *Proteoid*, *Ericaceous*, *Restiod* and *Asteraceous* growth forms (Cowling & Holmes 1992). The latter types of fynbos are primarily C_3 but contain some CAM and C_4 plants (Cowling & Holmes 1992). Fynbos occurs on the leached, oligotrophic soils derived from the Table Mountain Group sandstones but *Asteraceous* forms are also found on granites and shales of the Malmesbury & Bokkeveld Groups) (Bar-Matthews *et al.* 2010). Renosterveld occurs on the fertile shale-based soils of the Bokkeveld and Witteberg Groups and contains both C_3 and C_4 flora (Cowling & Richardson 1995). The extent of Renosterveld has been severely impacted through agricultural activities such as cattle grazing and wheat production (Cowling & Richardson 1995). Other vegetation types that may contribute to the speleothem $\delta^{13}\text{C}$ signal are the unique communities of thicket-type vegetation that comprises mainly C_4 and CAM plants. This subtropical dune thicket is supported by the calcretes and aeolianites of the coastal dunes.

The $\delta^{18}\text{O}$ composition of the speleothem calcite may be related to the temperature above the cave (Fairchild *et al.* 2006; McDermott *et al.* 2006; Sundqvist *et al.* 2007) and changes in the type and amount of precipitation (*e.g.* Baldini *et al.* 2005, 2006). In this study, a direct reconstruction of the palaeotemperatures during the growth of the *Blou1* and *KG2.3* speleothems is not possible. This is attributed to several factors. Firstly, both stalagmite samples were obtained from inactive caves with no modern drip water source and thus there is no analogue for calibrating the speleothem delta function (SDF) (see Chapter 4). Secondly, there is at present no suitable palaeotemperature proxy covering the interval represented by the *Blou1* and *KG2.3* stalagmites.

In a recent study undertaken at Crevice Cave in Pinnacle Point, some 150 km east of De Hoop Nature Reserve, Bar-Matthews *et al.* (2010) suggested that the speleothem $\delta^{18}\text{O}$ values were indicative of changes in the relative contribution of summer and winter rainfall. Depleted (*i.e.* lower) $\delta^{18}\text{O}$ values were associated with stronger winter rainfall whereas enriched (*i.e.* higher) $\delta^{18}\text{O}$ values were thought to reflect summer rain. The interpretation was based on the trends observed in the speleothem $\delta^{18}\text{O}$ signal, the $\delta^{18}\text{O}$ composition of modern drip water samples and the $\delta^{13}\text{C}$ profile of the Crevice Cave stalagmite.

This is by no means a straightforward interpretation as the $\delta^{18}\text{O}$ signal of precipitation is determined by the complex interplay of various factors. These include, amongst others, the amount and seasonality of rainfall, the percolation path of the drip water and evaporative effects (see Chapter 4 section 4.6).

In the De Hoop region, peak precipitation is received in winter (*viz.* August). Rainfall during the winter months is primarily associated with the temperate frontal systems embedded in the westerlies (Tyson & Preston-Whyte 2000; also see Chapter 2). Precipitation received during summer is by contrast, generated by the tropical components of the atmospheric circulation system as moisture is sourced from the warm Indian Ocean and the local coastal systems (Tyson & Preston-Whyte 2000; Chase & Meadows 2007). Variations observed in the De Hoop $\delta^{18}\text{O}$ values are therefore likely to reflect changes in both the *amount* and *type* of rainfall.

Holmgren *et al.* (2003) proposed that changes recorded in the $\delta^{18}\text{O}$ values of the Cold Air Cave stalagmite in the Makapansgat Valley of the South African interior, were related to shifts in the major components of the atmospheric circulation. More specifically, changes in the relative strength of the easterlies at the Intertropical Convergence Zone (ITCZ) and the westerlies. Rain-bearing cloud bands formed under either of these conditions (*i.e.* stronger/weaker easterlies & stronger/weaker westerlies) would consequently occur at different altitudes in the atmosphere.

Lower $\delta^{18}\text{O}$ values were associated with generally drier and colder conditions. The decrease in average annual rainfall which accompanied these cold intervals was associated with rainfall originating from clouds formed higher up in the atmosphere (*viz.* thunderstorm & hail clouds), a northward shift in the ITCZ and stronger westerlies (Holmgren *et al.* 2003 also Holzkämper *et al.* 2009). Higher $\delta^{18}\text{O}$ values were by contrast associated with warmer and wetter conditions with rain-bearing clouds formed at mid-altitudes caused by a southward shift in the ITCZ and weaker westerlies (Holmgren *et al.* 2003). Similar correlations have also been recorded at Wolkberg Cave in Limpopo, South Africa (Holzkämper *et al.* 2009).

It is within this context of changing atmospheric circulation patterns that the De Hoop $\delta^{18}\text{O}$ signal, which is represented by the *Blou1* and *KG2.3* samples, is interpreted. However, as the De Hoop region presently receives more rainfall in winter than in summer, lower $\delta^{18}\text{O}$ values may indicate generally cool conditions with more seasonal (winter) rainfall. Higher values are thought to indicate generally warm conditions with less seasonal precipitation. Interpretations of the De Hoop stable isotope signals, particularly the $\delta^{18}\text{O}$ profile, are rather complex. This is because the Indian Ocean sea surface temperatures (SSTs), tropical systems and westerly wind perturbations influence the climate of the southern Cape (Chase & Meadows 2007; Chase 2010). The stable isotope signal recorded in the Bloukrantz Cave (*Blou1*) and Kaisers Gat II (*KG2.3*) stalagmites, as described in this section, will be evaluated against other regional proxies, which are discussed further in Chapter 6.

5.3.1 *Blou1* $\delta^{13}\text{C}$ and $\delta^{18}\text{O}$ signal (Fig. 5.15)

Overall, higher $\delta^{13}\text{C}$ values are reflected in the (late) Holocene data of *Blou1* (see Fig. 5.9). The $\delta^{13}\text{C}$ values increased gradually from a minimum of -10 ‰ (when growth resumed after the hiatus) before reaching maximum values of -3.3 ‰ by *c.* 3.5 ka. The $\delta^{13}\text{C}$ signal at 3.5 ka is broadly congruent with the Cango Cave stalagmite record correlated with the period between 0 and 2 kBP (Talma & Vogel 1992). C_4 vegetation estimates from this cave, located some 300 km northwest of De Hoop, equate the

Blou1 $\delta^{13}\text{C}$ data to *c.* 70 % C_4 and 30 % C_3 . The extant vegetation in De Hoop is lowland fynbos, which has a C_3 isotopic signal. The *Blou1* values by contrast indicate a stronger C_4 and perhaps CAM vegetation component in the vicinity at *c.* 4 ka. A related post-hiatus pattern was observed in the $\delta^{18}\text{O}$ signal with values increasing from -5 ‰ to -3 ‰. In the *Blou1* record, these relatively enriched isotope values reflect a shift towards drier conditions that is concurrent with changes in the mineralogy (*viz.* aragonite) noted in the upper part of the *Blou1* stalagmite. In the present study however interpretations of the *Blou1* Holocene data is considered tentative. The main reason for this is that aragonite and calcite are geochemically different and higher $\delta^{18}\text{O}$ and $\delta^{13}\text{C}$ values are typically associated with aragonite (*e.g.* Frisia *et al.* 2002; McMillan *et al.* 2005). For comparative purposes, standard corrections are generally applied to account for the fractionation between calcite and aragonite (*e.g.* Holmgren *et al.* 2003). Although the *Blou1* isotopic values were not corrected for aragonite, the deposition of aragonite is thought to reflect drier conditions above the cave.

In the period between 48 and 46 ka changes were observed in both the $\delta^{13}\text{C}$ and $\delta^{18}\text{O}$ values. The $\delta^{13}\text{C}$ values varied between -5 and -1 ‰ and the corresponding $\delta^{18}\text{O}$ values between -2.5 and -1.5 ‰. Overall, the $\delta^{13}\text{C}$ values represent a trend of gradually increasing C_4 and possibly CAM plant (*viz.* geophyte) dominance, which correlated with generally warmer conditions and perhaps reduced precipitation as inferred from the $\delta^{18}\text{O}$ signal. This is contrary to the trends observed in the Crevice Cave stalagmite record (Bar-Matthews *et al.* 2010). At this site, the $\delta^{13}\text{C}$ and $\delta^{18}\text{O}$ values were thought to reflect more C_4 vegetation and warmer rain near Pinnacle Point from *c.* 66 to 50 ka (Bar-Matthews *et al.* 2010). Based on the formation of the flowstone in Kaisers Gat II (KG2.2) it is possible that moister conditions may have been prevalent in the De Hoop region *c.* 50 ka. This is because flowstones typically develop under conditions of higher effective precipitation (*e.g.* Ayliffe *et al.* 1998; Hodge *et al.* 2008). Unfortunately, uncertainties regarding the age of this flowstone prevent any firm interpretations from being made.

In the *Blou1* record, stable isotope values declined sharply by the onset of the hiatus *c.* 45 ka. The apparent hiatus persisted until growth resumed in the late Holocene (*c.* 3.5 ka). A contemporaneous break in carbonate precipitation *c.* 46-40 ka is reported in the Wolkberg Cave stalagmite, which is located *c.* 1775 km southwest of De Hoop (Holzkämper *et al.* 2009). The implication is that the hiatus identified in the *Blou1* record may reflect regional climatic changes.

5.3.2 KG2.3 $\delta^{13}\text{C}$ and $\delta^{18}\text{O}$ signal (Fig. 5.16)

The KG2.3 record falls broadly in the period from *c.* 100 to *c.* 115 ka within the interstadial of MIS 5c and the stadial of MIS 5d. Globally, the last interglacial is associated with rapid climatic oscillations and corresponding changes in temperature and sea level. The abrupt fluctuations characterising this marine isotope stage are to some extent reflected in the variations of the $\delta^{13}\text{C}$ and $\delta^{18}\text{O}$ values around the respective mean values of -9.1 ‰ and 2.6 ‰ (Fig. 5.16). Based on the variations of the $\delta^{13}\text{C}$ values around the mean of -9.1 ‰ it appears that vegetation comprising C_3 , C_4 and possibly CAM types may have been present in the vicinity during the growth of the KG2.3 stalagmite. The rapid, small amplitude fluctuations observed in the $\delta^{18}\text{O}$ values around the mean of -2.6 ‰ fall within the range of warmer rainfall recorded at Crevice Cave (Bar-Matthews *et al.* 2010) (Fig. 5.16). Overall, the KG2.3 $\delta^{18}\text{O}$ record indicates that conditions were generally warmer and perhaps wetter between *c.* 100-*c.* 115 ka. Conditions with sufficient moisture for speleothem growth during this period are also inferred from the deposition of humic-rich laminations and visible pores observed in this sample. These features are thought to reflect relatively fast and possibly continuous growth. However, interpretations of the $\delta^{18}\text{O}$ signal in the KG2.3 record are constrained by the absence of modern drip water samples and the uncertainties regarding its stratigraphy. In Chapter 6, this record is assessed further using other regional proxies.

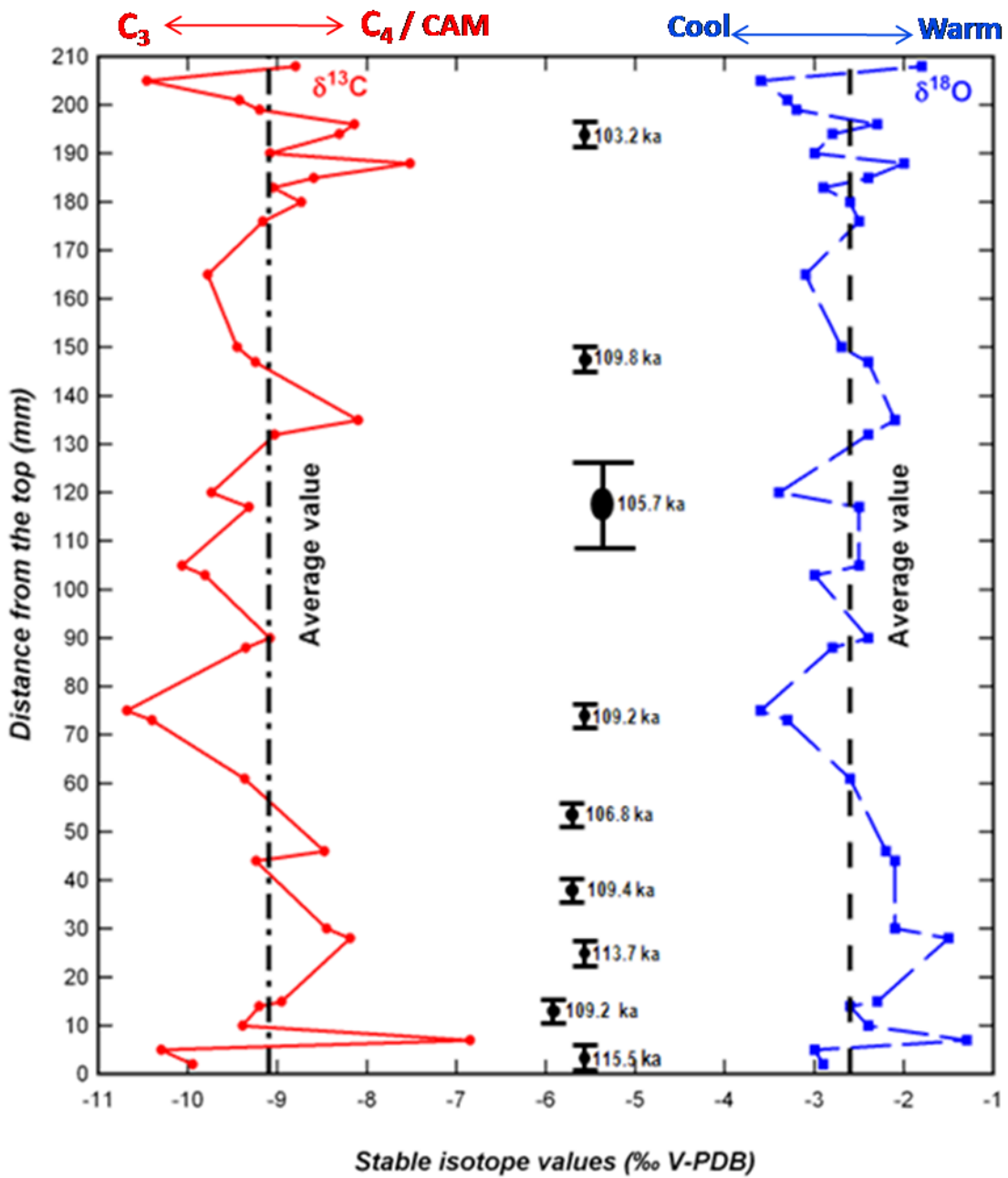


Figure 5.16 $\delta^{13}\text{C}$ and $\delta^{18}\text{O}$ values and uncorrected U-series ages obtained for the KG2.3 sample. The ages are not interpolated because of the discrepancy between the stratigraphy and corresponding age determinations

5.4 Summary

The *Bloul* stalagmite provides a discontinuous record from *c.* 48-46 ka with a hiatus in stalagmite growth from *c.* 45 ka until the late Holocene *c.* 3.5 ka. The Holocene vegetation signal is characterised by stronger C₄ and weaker C₃ vegetation types, which are associated respectively, with high and low $\delta^{13}\text{C}$ values. It is possible that the C₄ signal includes a contribution from CAM plants, (which may have included geophyte species and small succulents) as the isotopic signal of CAM plants is often very similar to that of C₄ plants (Keeley & Rundel 2003). The corresponding $\delta^{18}\text{O}$ values indicate slightly cooler conditions that are concurrent with changes in the deposition of aragonite in the upper part of the *Bloul* stalagmite.

In the interval between 46 and 48 ka the vegetation comprised mainly C₄ plant types and may have included grasses, CAM and possibly dune thicket elements. The presence of C₄ vegetation during this period correlates with higher $\delta^{18}\text{O}$ values (*c.* -2.5 ‰ to -1.0 ‰). These isotopic values are thought to represent warm conditions with a progressive decrease in moisture availability which coincides with the termination of stalagmite growth *c.* 45 ka.

The general pattern observed in the *KG2.3* $\delta^{18}\text{O}$ record is that conditions above the Kaisers Gat II cave were warmer throughout the growth of this stalagmite. The corresponding $\delta^{13}\text{C}$ values suggests a mosaic of C₃, C₄ and possibly CAM vegetation types were prevalent in the region from *c.* 100- *c.* 115 ka. These interpretations are however tentative as the ambiguous stratigraphy of the *KG2.3* sample resulted in the average isotopic signal being used for interpretative purposes.

Figures 5.17 and 5.18 provide an illustrative summary of the $\delta^{13}\text{C}$ and $\delta^{18}\text{O}$ isotopic signals preserved in the *Bloul* and *KG2.3* stalagmites. Although these isotope records do not cover the Still Bay occupation at Blombos Cave, the *KG2.3* record appears to fall within the M3 phase of Middle Stone Age occupation at the site. The De Hoop isotope record therefore allows for general interpretations about the environment and

archaeology during the *c.* 100 ka M3 occupation at the Blombos site. The discussion in Chapter 6 explores this further.

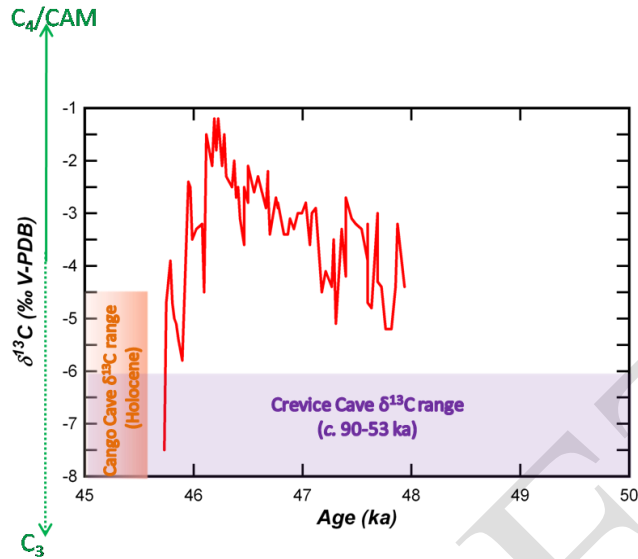


Figure 5.17 $\delta^{13}\text{C}$ time-series for *Blou1*

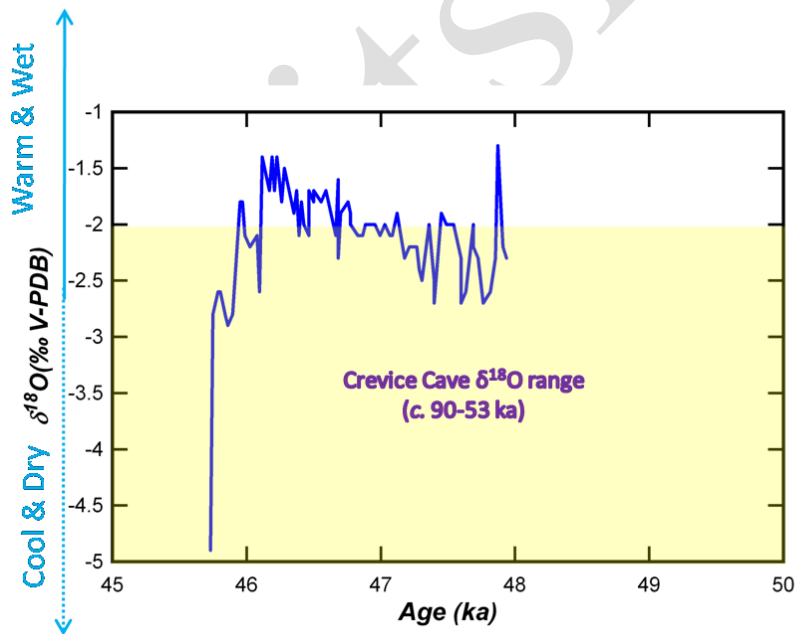


Figure 5.18 $\delta^{18}\text{O}$ isotope record for *Blou1*